Hybrid simulations of extensive air showers

Jaime Alvarez-Muñiz,* Ralph Engel, T. K. Gaisser, Jeferson A. Ortiz,† and Todor Stanev‡
Bartol Research Institute, University of Delaware, Newark, Delaware 19716
(Received 22 May 2002; published 29 August 2002)

We present a fast one dimensional hybrid method to efficiently simulate extensive air showers up to the highest observed energies. Based on precalculated pion showers and a bootstrap technique, our method predicts the average shower profile, the number of muons at detector level above several energy thresholds as well as the fluctuations of the electromagnetic and hadronic components of the shower. We study the main characteristics of proton-induced air showers up to ultra high energy, comparing the predictions of three different hadronic interaction models: SIBYLL 1.7, SIBYLL 2.1 and QGSJET98. The influence of the hadronic interaction models on the shower evolution, in particular the elongation rate, is discussed and the applicability of analytical approximations is investigated.

DOI: 10.1103/PhysRevD.66.033011 PACS number(s): 96.40.Pq, 13.85.−t

I. INTRODUCTION

Extensive air showers (EAS) generated by cosmic rays in the Earth's atmosphere are the only way to study cosmic rays of energies above 10^{15} eV. At lower energies the cosmic ray spectrum and composition are studied in experiments that measure directly the charge and energy of the primary particle. The analysis of air shower data relies on simulations that use the current knowledge of hadronic interactions to predict the observable shower parameters. With increasing cosmic ray energy, this task becomes more difficult as the gap between the shower energy and the energy range studied in accelerator experiments increases and the hadronic interaction properties have to be extrapolated over a wide range. The difficulties are also related to the fact that particles produced in the forward region of the interaction are not registered in collider experiments, while they are responsible for most of the shower characteristics. Last but not least, the atmospheric targets are light nuclei which have not been studied in collider experiments.

Air shower experiments are either ground arrays of detectors that trigger in coincidence when the shower passes through them, or optical detectors that observe the longitudinal development of EAS. Both types of instruments are sometimes supplemented by shielded or underground detectors that observe the muon component of the showers. The most commonly observed EAS parameters are the number of charged particles at ground level for the shower arrays, or at shower maximum ($S_{\max}$) for the optical detectors; the depth of shower maximum ($X_{\max}$) itself; and the number of muons (N_{μ}) above different energy thresholds. The combination of these and occasionally additional shower features, calculated in simulations with a particular hadronic model, is used as the basis for the determination of the energy and mass of the primary particle. Reviews of air shower experiments and observed features are given, for example, in [1,2].

At the end of the cosmic ray spectrum, at energies above 10^{19} eV, air shower simulation becomes a very difficult problem technically. The number of charged particles that have to be followed in the Monte Carlo scheme is proportional to the shower energy. For example, highest energy cosmic ray showers [3,4] can have more than 10^{11} charged particles at $X_{\max}$. As a consequence the direct simulation of the shower following each individual particle becomes practically impossible, especially when a large number of showers has to be simulated.

The widely used solution to the problem of having to deal with an excessively large number of shower particles is the simulation of EAS using the thinning technique [5]. This method is extremely useful to estimate detectable signals and to compute average values of the observables [6,7]. The thinning procedure follows only a subset of the shower particles below a certain energy threshold, assigning weights to them so that the average number of particles at the ground is correctly reproduced. Because of this, artificial fluctuations are introduced even when small energy thresholds are used. Various methods of reducing artificial fluctuations have been proposed recently (e.g. [8,9]) optimizing the compromise between time-consuming simulations and fluctuation-enhancing thinning.

In this work we present a hybrid method of simulating the longitudinal profile of extensive air showers. It is a fast, one dimensional calculation which provides predictions for the total number of charged particles and muons along the shower axis. The method allows the collection of sufficiently high Monte Carlo statistics without losing information about shower fluctuations.

In general, hybrid calculations are based on the idea to follow the development of air showers in detail above a certain energy threshold and to replace subthreshold particles by a simplified and efficient approximation of the subshowers initiated by them. Many hybrid calculations use the Monte Carlo–generated high-energy secondary particles of the first few interactions of a cosmic ray in the atmosphere as initial distribution, and then calculate the particle densities observed at detector level by solving the corresponding transport equations (see, for example, [10–15]).

*Electronic address: alvarez@bartol.udel.edu
†Also at Instituto de Física "Gleb Wataghin," Universidade Estadual de Campinas, 13083-970 Campinas-SP, Brazil.
‡Also at Laboratoire de Physique Corpusculaire et Cosmologie, Collège de France, Paris, France.

Here we follow the approach of Gaisser *et al.* [16] and treat the subthreshold particles with a library of shower profiles based on presimulated pion-initiated showers. This idea can be combined in a bootstrap procedure [17] to extend the shower library to high energy. The novelty of this work is that we extend the method of [16,17] by accounting for fluctuations in the subshowers generated with the shower library, and also calculate the number of muons at detector level above several energy thresholds.

Showers simulated in this way can be used as input to simulations for experiments measuring the longitudinal development of the shower such as HiRes [18], the fluorescence detector of the Pierre Auger Observatory [19] and future experiments such as EUSO [20], OWL/AirWatch [21] and the Telescope Array [22]. Besides this, as will become clear later, hybrid simulations are very helpful for comparing shower parameters predicted by different hadronic interaction models and to aid the interpretation of the experimental results in this way.

This paper is structured as follows. In Sec. II we describe the hybrid method and the parametrizations of the presimulated showers. We demonstrate the self-consistency of the method by comparing showers simulated directly with predictions from the hybrid calculation. In Sec. III we apply the hybrid method to proton induced showers at fixed energy. We give the average values and distributions of $X_{\max}$, $S_{\max}$, and N_{μ} obtained for different hadronic models and discuss how the differences are related to the simulation of high-energy multiparticle production. In addition the elongation rate theorem [23,24] is discussed in terms of the different hadronic interaction models and their influence on the position of the shower maximum. Where available, we compare our predictions to calculations performed with the CORSIKA code [25] which uses the thinning approach. Section IV summarizes our results and concludes the paper.

II. THE HYBRID METHOD

The hybrid method used in this work consists of calculating shower observables by a direct simulation of the initial part of the shower, tracking all particles of energy $>fE$, where E is the primary energy and f is an appropriate fraction of it (in the following we use $f=0.01$). Then presimulated showers for all subthreshold particles are superimposed after their first interaction point is simulated. The subshowers are described with parametrizations that give the correct average behavior and at the same time describe the fluctuations in shower development. The method is extended recursively to higher energies: the results obtained at any primary energy are used for the simulation of showers at higher energy.

It is well known that the fluctuations in shower properties are dominated by fluctuations in the earliest and most energetic part of the cascade. We however parametrize both the average behavior and the shower fluctuations starting at 10 GeV. In this way we can use the hybrid method at relatively low energy of 100 – 1000 TeV, where the results can be compared to those of direct (fully simulated) shower calculations.

We build a library of presimulated showers by injecting pions of fixed energy E_{π}, at fixed zenith angle θ and depth X measured along the shower axis. The atmospheric density adopted here corresponds to Shibata's fit of the U.S. Standard Atmosphere [26,27], very similar to Linsley's parametrization. We limit the injection zenith angles to $\theta<45°$ since mainly showers in this angular range have been used for studies of the cosmic ray energy spectrum at the highest energies.

Nucleon initiated showers are not presimulated. Nucleons are followed explicitly in the Monte Carlo simulation down to the energy threshold for particle production. A subshower initiated by a kaon is assumed to be similar to one initiated by a pion of the same energy but with a different first interaction point, which is sampled from the corresponding interaction length distribution. This approximation is not expected to affect significantly our final results, the main reasons being the similarity between pion and kaon induced showers at high energy combined with the fact that the main contribution to shower development in this method comes from the highest energy particles that enter the parametrizations. Unstable particles, including π^0, η, Λ, Σ and Ω are allowed to interact or decay in the code. The interaction of these particles becomes important at the highest energies and accounting for them can influence the average values of some observables.

Photon and electron/positron induced cascades are treated with a full screening electromagnetic Monte Carlo simulation in combination with a modified Greisen parametrization. The electromagnetic branch of the Monte Carlo simulation includes photoproduction of hadrons. For energies above 1 EeV, the Landau-Pomeranchuk-Migdal (LPM) effect [28–31] is taken into account using an implementation by Vankov [32]. The influence of the geomagnetic field on the cascade development [33] is neglected.

We have simulated primary pions of energies between 10 GeV and 3 EeV with a step in energy of half a decade, interacting at fixed atmospheric depths $X_0=5,50,100,200,500$ and 800 g/cm^2. For each pion energy, injection zenith angle and depth (i.e. a single entry in the library) we simulate 10 000 showers (5000 at high energy) and record $X_{\max}$, $S_{\max}$, the longitudinal shower profile, and the number of muons above the threshold energies of 0.3, 1, 3, 10 and 30 GeV both at sea level and at a depth of 400 g/cm^2 above sea level measured along the shower axis. These values are used to produce distributions of showers in $X_{\max}$ and $S_{\max}$, the correlations between them and distributions of the number of muons at sea level. The whole procedure of generating a library has to be carried out for each of the interaction models we adopt in this work (see Sec. III A).

Figure 1 shows an example of the correlation between $X_{\max}$ and $S_{\max}$. The plot contains 5000 simulated pion showers of energy 3.16×10^{18} eV initiated at an atmospheric depth of $X_0=5$ g/cm^2 and zenith angle $\theta=45°$. Correlations similar to these are produced for each entry in the library. Their correct representation is crucial for the successful modeling of shower fluctuations.

Although it is unlikely to produce a high energy pion deep in the atmosphere, we also calculate their interactions at depths as large as 500 and 800 g/cm^2 to obtain an accurate

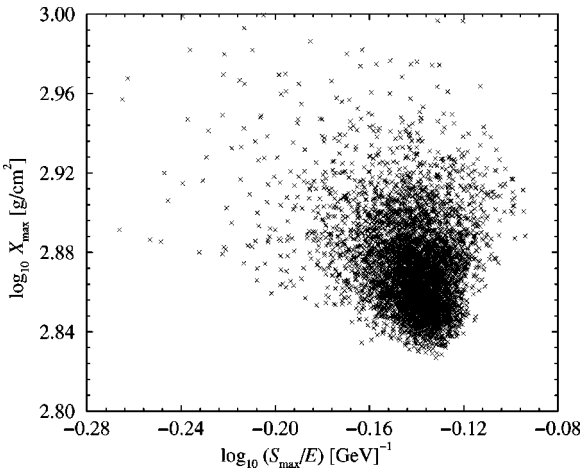

FIG. 1. The correlation between $\lg X_{\max}$ and $\lg S_{\max}$ for 5000 pion induced showers at primary energy 3×10^{18} eV initiated at $X_0=5$ g/cm^2 and zenith angle $\theta=45°$.

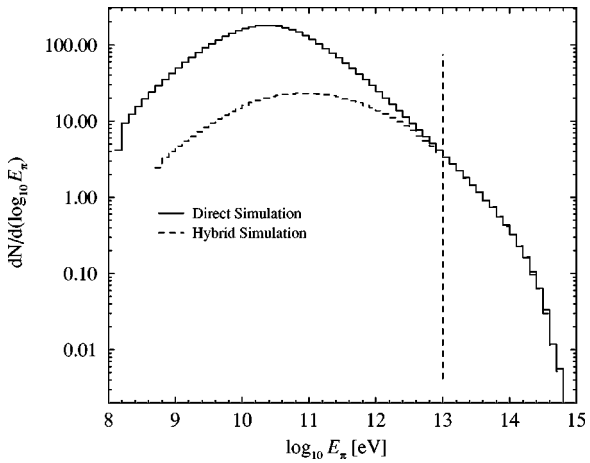

FIG. 2. Energy distribution of pions in showers initiated by primary protons at $E=10^{15}$ eV. The dashed curve is the energy distribution of the pions actually treated in our hybrid simulation procedure using a hybrid energy threshold of 10^{13} eV. The solid curve shows the energy distribution of pions which are explicitly tracked in a direct simulation. Pions which decay are not shown.

description of the muon numbers at sea level and a better description of the late developing electromagnetic showers. For showers initiated after 500 g/cm^2 the atmosphere has been artificially extended beyond ground level. The distributions of muons are easily extended to other depths (corresponding to the observation level of different experiments) by extrapolation. For this task we use the slope of the muon longitudinal profile between sea level and a slant depth of 400 g/cm^2 above sea level.

The longitudinal development of subthreshold meson induced showers is parametrized using a slightly modified version of the well-known Gaisser-Hillas function that gives the number of charged particles at atmospheric depth X [34]:

$$S_{\mathrm{GH}}(X)=S_{\max}\left(\frac{X-X_0}{X_{\max}-X_0}\right)^{(X_{\max}-X_0)/\lambda(X)} \times\exp\left[-\frac{(X-X_{\max})}{\lambda(X)}\right]. \quad (1)$$

Here $\lambda(X)=\lambda_0+bX+cX^2$ where λ_0, b and c are treated as free parameters. X_0 is the depth at which the first interaction occurs. The parameters b and c are assumed to be the same for all showers initiated at a given depth, angle, and energy. They are determined by fitting the mean shower profile of the parametrized showers to that obtained from the simulated shower profiles.

The innovative approach of our method is that instead of using the average values of $X_{\max}$ and $S_{\max}$ to generate subthreshold meson showers of a certain energy, we sample their values (as well as the number of muons) from their corresponding presimulated distributions, taking into account the correlation between them (Fig. 1). This procedure accounts for the fluctuations in the subshower development. A technical remark is that we sample the observables directly from their precalculated histograms, i.e. we do not assume any functional form for the distribution. In this way our code is very flexible—it allows the study of hadronic models that predict distributions of observables not easily fitted by analytical functions.

We sample meson subshowers at a zenith angle, depth and/or primary energy different from those we have presimulated by interpolating between the relevant parameters of the shower development $(X_{\max},S_{\max},\lambda_0,b,c,N_\mu)$, corresponding to presimulated entries in the library which are adjacent in angle, energy, and depth to the subshower we want to describe. We have experimented with different types of interpolation which were motivated by the behavior of the parameters with energy, depth, and zenith angle, and we have adopted those which produce the smallest discrepancies between fully simulated showers and showers obtained with our hybrid method. The interpolation in energy of $X_{\max},\log_{10}S_{\max},\lambda_0,b,c$ and $\log_{10}N_\mu$ is in $\log_{10}E$, while the interpolation in X_0 and $\cos\theta$ is linear or the closest neighbor is used.

In Fig. 2 we plot the energy distribution of pions actually treated in our hybrid simulation procedure (dashed line). For comparison we also show the energy distribution of pions that must be explicitly tracked in a direct simulation (solid line) at the same energy. The comparison is made for $E=10^{15}$ eV proton induced showers and for the nominal energy threshold of 0.01 E. In the hybrid approach only the interactions of pions above 0.01 E are directly simulated and all lower energy pions are replaced with parametrizations. For a primary energy 10^{15} eV we typically treat 1 out of 10 pions of energy $\sim3\times10^{10}$ eV as can be obtained from the figure. This explains the saving in CPU time achieved with the hybrid code with respect to the direct simulation—a factor about 7 for the particular energy shown here. This factor rapidly increases with energy. Already at $E=10^{16}$ eV the hybrid calculation is about 25 times faster than a direct simulation (Table I). For applications which do not depend on the number of muons this factor increases even further. At

TABLE I. Average values of different observables and standard deviation of their distributions obtained by direct and hybrid simulations of 5000 vertical pion showers with fixed interaction point $X_0=5$ g/cm^2, and primary energy $E=10^{16}$ eV. The predictions of SIBYLL .7, SIBYLL 2.1 and QGSJET98 are presented. The energy threshold in the hybrid calculation is $0.01\ E=10^{14}$ eV.

	SIBYLL 1.7		SIBYLL 2.1		QGSJET98	
Model	Direct	Hybrid	Direct	Hybrid	Direct	Hybrid
$\langle X_{\max}\rangle$[g/cm^2]	603	602	587	586	574	576
$\sigma(X_{\max})$[g/cm^2]	49	50	51	49	55	56
$\langle S_{\max}\rangle/E$[GeV^{-1}]	0.75	0.76	0.75	0.75	0.75	0.75
$\sigma(S_{\max}/E)$[GeV^{-1}]	6.8×10^{-2}	6.8×10^{-2}	6.3×10^{-2}	6.2×10^{-2}	6.5×10^{-2}	6.5×10^{-2}
$\langle N_\mu\rangle(>0.3$ GeV)	5.39×10^4	5.41×10^4	6.10×10^4	6.13×10^4	6.87×10^4	6.91×10^4
$\sigma(N_\mu)$	1.79×10^4	1.81×10^4	1.86×10^4	1.87×10^4	2.25×10^4	2.28×10^4
CPU Time [min]	935	33	1091	41	1398	79

[a]All CPU times illustrated in this work refer to a 1 GHz AMD Athlon processor.

10^{15} eV about 25% of the CPU time is spent on correctly tracking the numerous muons that are decay products of charged pions and kaons which do not initiate hadronic showers, and hence do not enter the parametrizations. With increasing energy the number of mesons which decay at an energy above the hybrid threshold decreases, and the number of muons which have to be simulated explicitly becomes negligible.

To ensure the consistency of our simulation approach, we have compared full simulations of pion showers to hybrid simulations for the same initial energy and depth using several energy thresholds. We find a very good agreement between the average values of the different observables and their fluctuations in the direct and hybrid simulations. Table I compares the direct simulations and the hybrid method for 5000 vertical pion showers with fixed first interaction point at $X_0=5$ g/cm^2, energy 10^{16} eV, and for the different hadronic models. It is very important to note that the differences between the two methods of calculation are much smaller than those introduced by the different hadronic interaction models, i.e. by using the hybrid approach we do not lose sensitivity to the models we are considering.

In Fig. 3 we plot the distribution of the number of muons with energy above 0.3 GeV at sea level for vertical pion-induced showers of energy 10^{16} eV. We compare the direct simulation to the results of the hybrid approximation. Panel (a) shows this comparison for QGSJET98 and panels (b) and (c) are for SIBYLL 2.1 and SIBYLL 1.7, respectively. The relative differences in the average number of muons are less than 0.5% for all hadronic interaction models. The same comparison for showers generated by primary pions with an incident zenith angle of 45° shows larger differences between direct and hybrid simulations, but they are smaller than 2%. We believe these relatively small errors come mostly from the representation of the intrinsic fluctuations in the shower development and from the interpolation in energy and atmospheric depth that the code performs. Due to the bootstrap-like calculation of the high-energy part of the library this error increases slowly with energy. Comparisons with direct simulations at 10^{18} eV show that the deviations in the average number of muons is typically 4%. Even for QGSJET98, which predicts the largest fluctuations at this energy, we obtain a very good description of the distributions. Their width is reproduced with an error smaller than 3%. For proton-induced showers the hybrid code always tends to underestimate the number of muons and its fluctuations.

Our results also show a remarkable stability under changes of the energy threshold, from which we conclude that the primary to threshold energy ratio we have used ($E_{\rm thr}=E/100$) is sufficient to achieve a very good description of the average values and fluctuations of observables in nucleon and pion initiated showers. Using a threshold for

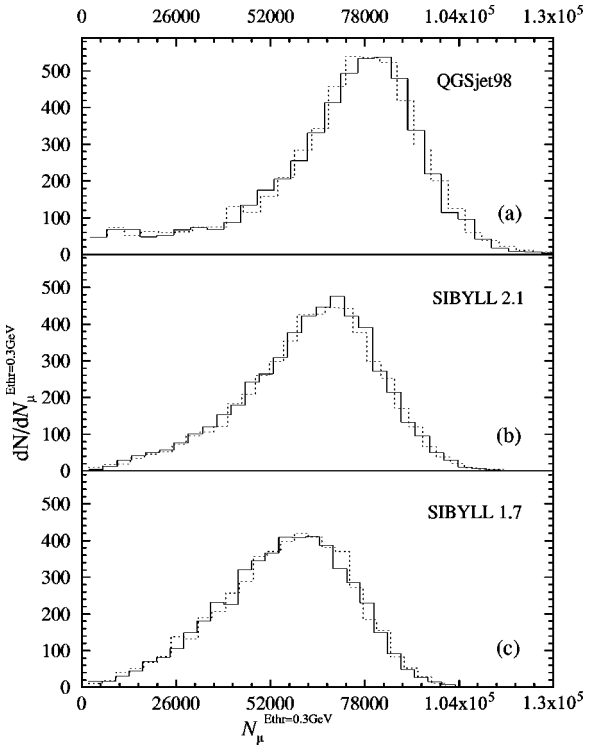

FIG. 3. Shower distribution in number of muons of energy above 0.3 GeV at sea level. Results are shown for 5000 vertical pion-initiated showers of energy $E=10^{16}$ eV, at fixed interaction point $X_0=5$ g/cm^2 for different hadronic models. The solid line represents fully simulated showers while the dotted line shows hybridly simulated showers with meson energy threshold $E/100$.

mesons and for the electromagnetic component fixed to $E_{\rm thr}^{\rm em}=E_{\rm thr}^{\rm mes}=E/10$, we still obtain a good agreement for the average values. However we might not correctly include some of the extreme fluctuations that are possible in the early development of the showers.

III. APPLICATIONS

In this section we apply the hybrid approach described above to simulate proton-initiated showers at fixed energy. These showers show most transparently the influence of the hadronic interaction model on air shower observables. In a forthcoming paper we will calculate predictions for a realistic cosmic ray spectrum with a mixed cosmic ray composition consisting of protons and nuclei [35].

In the following we consider the hadronic interaction models SIBYLL and QGSJET. We have created libraries for the model versions SIBYLL 1.7 [36], SIBYLL 2.1 [37,38] and QGSJET98 [39]. QGSJET and SIBYLL are sufficiently different to illustrate various important points of how properties of hadronic interactions are reflected in shower observables. In addition they are commonly used for the analysis of air shower measurements. In discussing the models we will focus on QGSJET98 and SIBYLL 2.1 and show SIBYLL 1.7 predictions only for reference purposes because many air shower data have been already analyzed with this model.

SIBYLL 2.1 shows a considerable improvement with respect to version 1.7 in describing the measurements of hadronic interactions at collider energies. The important changes in SIBYLL are the implementation of new parton densities and parton saturation, a new model for diffraction dissociation, and an energy-dependent soft component [37]. Nevertheless, at the highest cosmic ray energies, its predictions are similar to those of SIBYLL 1.7. On the other hand, QGSJET98 predicts a high-energy extrapolation which is strikingly different from that of SIBYLL.

A. Hadronic interaction models

QGSJET98 and SIBYLL 2.1 were shown to describe well collider data up to the highest energies available so far (see for instance [40]). However, already the extrapolation to the unmeasured parts of the phase space is different. These differences are amplified by going from proton-proton to proton-air collisions.

One of the key features of the hadronic interaction models is their prediction on hadron-air cross sections. The proton-air cross section determines the height of the first interaction in the atmosphere. However, it should be emphasized that the pion- and kaon-air cross sections are also very important for the shower development. Figure 4 shows the model cross sections for proton- and pion-proton collisions which are the input for the calculation of hadron-air cross sections. In both models free parameters are adjusted to fit the measured pp and $p\bar{p}$ cross sections which cover the energy range from the low end up to $E_{\rm lab}\approx 1.7\times 10^{15}$ eV, i.e. Tevatron center-of-mass energy of $\sqrt{s}=1800$ GeV. The model predictions for the pion-proton cross section diverge already at much lower energy. The experimental restrictions here are much smaller

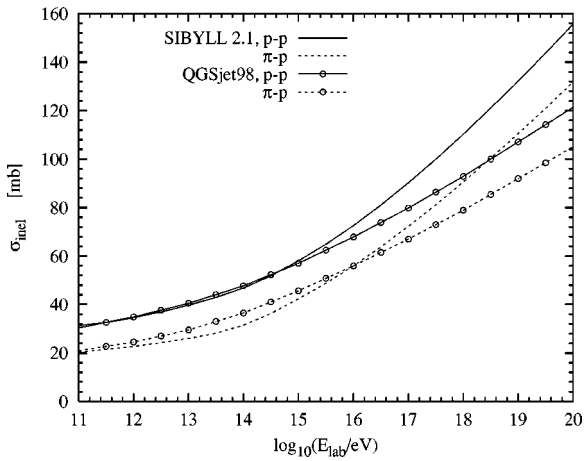

FIG. 4. Inelastic proton-proton and pion-proton cross sections as predicted by QGSJET98 and SIBYLL.

since the pion-proton cross section is experimentally known only up to $E_{\rm lab}=4\times 10^{11}$ eV. The difference in the high-energy extrapolation of the models arises from different assumptions on the spatial distribution of partons in protons and pions. Both models implement the eikonal approximation but differ in many technical details such as the treatment of inelastic diffraction. In the following we discuss only the most basic version of the eikonal model as it is sufficient for explaining the important differences.

In the eikonal model the inelastic cross section is given by

$$\sigma_{\rm inel}=\int d^2\vec{b}[1-\exp\{-2\chi_s(s,\vec{b})-2\chi_h(s,\vec{b})\}], \quad (2)$$

where the eikonal function is written as the sum of soft and hard contributions, χ_s and χ_h. The two-dimensional impact parameter of the collision and the squared center-of-mass energy of the collision are denoted by $\vec{b}$ and s. At high energy one has $\chi_h \gg \chi_s$ and the inelastic cross section is dominated by χ_h, written as

$$\chi_h(s,\vec{b})=\tfrac{1}{2}\,\sigma_{\rm QCD}(p_\perp^{\rm cutoff},s)A(s,b), \int d^2\vec{b}A(s,b)=1. \quad (3)$$

The normalized profile function $A(s,b)$ describes the distribution of partons in the plane transverse to the collision axis. The minijet cross section $\sigma_{\rm QCD}$ depends on the collision energy and the transverse momentum cutoff, $p_\perp^{\rm cutoff}$, needed to restrict the calculation to the perturbative region. For a given energy dependence of the minijet cross section, only the profile function $A(s,b)$ determines the inelastic cross section and its energy dependence.

Qualitatively, QGSJET is a model which assumes a Gaussian profile function [41]

$$A(s,\vec{b})=\frac{1}{\pi R^2}\exp\left\{-\frac{\vec{b}^2}{R^2}\right\}, \quad (4)$$

with R being a parameter. The SIBYLL model is based on the Fourier transform of the electromagnetic form factor, assum-

ing that the distribution of gluons in a hadron is similar to that of the quarks. The corresponding profile function is energy-independent and is, for example, for proton-proton scattering [36]

$$A(\vec{b}) = \frac{\nu^2}{96\pi}(\nu|\vec{b}|)^3 K_3(\nu|\vec{b}|), \tag{5}$$

where K_3 denotes the modified Bessel function of the third kind and $\nu \approx 0.7-1$ GeV^{-1}.

For all $|\vec{b}| < b_s$ with $\chi_h(s,b_s) \gg 1$ the saturation limit is reached. From Eq. (2) it follows that any further increase of the minijet cross section would not change the contribution to the cross section integral from the impact parameter region $|\vec{b}| < b_s$. This allows us to give a rough estimate of the energy dependence of the inelastic cross section at very high energy. For a QCD cross section dependence of $\sigma_{\rm QCD} \sim s^{\Delta}$, as is expected within perturbative QCD [42], one gets for a Gaussian profile

$$b_s^2 \sim R^2 \Delta \ln s \tag{6}$$

and at high energy

$$\sigma_{\rm inel} \approx \int d^2\vec{b}\,\theta(b_s - b) = \pi R^2 \Delta \ln s. \tag{7}$$

For R being energy-independent the cross section will rise only logarithmically with the collision energy. However, the parameter R itself depends on the collision energy through a convolution with the parton momentum fractions, $R^2 \approx R_0^2 + 4\alpha'_{\rm eff} \ln s$ and $\alpha'_{\rm eff} \approx 0.11$ GeV^{-2}. Hence the QGSJET cross section exhibits a faster than $\ln s$ rise

$$\sigma_{\rm inel} \sim 4\pi\Delta\alpha'_{\rm eff} \ln^2 s. \tag{8}$$

The cross section limit for SIBYLL can be derived in the same way from Eq. (5)

$$\sigma_{\rm inel} \sim \pi c \frac{\Delta^2}{\nu^2} \ln^2 s, \tag{9}$$

where the coefficient $c \approx 2.5$ was found numerically.

Both cross sections satisfy the Froissart bound and exhibit a $\ln^2 s$ energy dependence. However, the numerical factors are different. Assuming $\Delta \approx 0.25$, then $4\pi\alpha'_{\rm eff}\Delta \approx 0.13$ mb and $c\pi\Delta^2/\nu^2 \approx 0.2$ mb, which explains the faster increase of the inelastic cross section in the SIBYLL model. A larger power of $\Delta \approx 0.4$, as implied by data from the HERA collider [43], even amplifies the model differences. However, the difference between the model predictions is smaller than expected from the arguments above, the reason being a somewhat smaller minijet cross section assumed in SIBYLL as compared to QGSJET. The saturation of the parton densities implemented in SIBYLL tames their rapid growth at small parton momentum [37].

Information on the profile function can be derived by comparing the differential elastic cross sections measured at accelerators with model predictions [44,45]. The form factor approach describes current data reasonably well [46], whereas a Gaussian profile shows large, systematic deviations and predicts a wrong curvature. Although currently available data clearly favor profile functions derived from electromagnetic form factors, it is not clear whether this approximation is still good at ultrahigh energy.

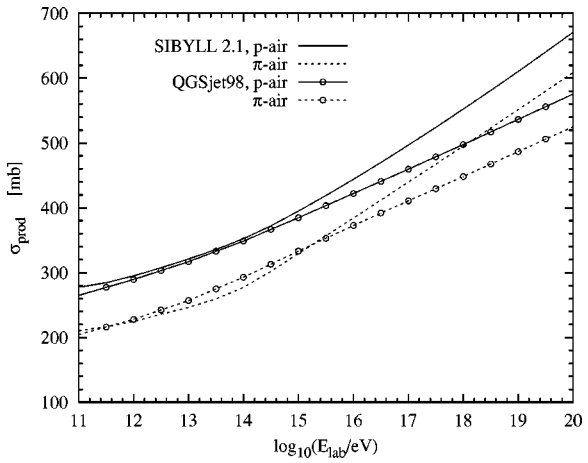

FIG. 5. Proton- and pion-air production cross section. The production cross section is defined as the cross section for all collisions in which at least one new particle is produced. It can be written as $\sigma_{\rm prod} = \sigma_{\rm tot} - \sigma_{\rm el} - \sigma_{\rm qel}$ where $\sigma_{\rm tot}$ is the total cross section and $\sigma_{\rm el}$ and $\sigma_{\rm qel}$ are the elastic and quasi-elastic cross sections respectively.

For hadron-air collisions (Fig. 5) the relative uncertainty in the extrapolated cross sections is considerably smaller than that of proton-proton and pion-proton cross sections. The geometrically large size of the target nucleus (mainly nitrogen or oxygen) dominates the interaction cross section. At the highest energy considered here the relative difference is less than 15%.

The evolution of air showers in the atmosphere depends directly on how much energy is transferred in each hadron interaction into the electromagnetic component of the shower. It is common to describe this energy transfer in terms of the elasticity of the interaction. Figure 6 shows the mean elasticity of proton- and pion-air interactions as pre-

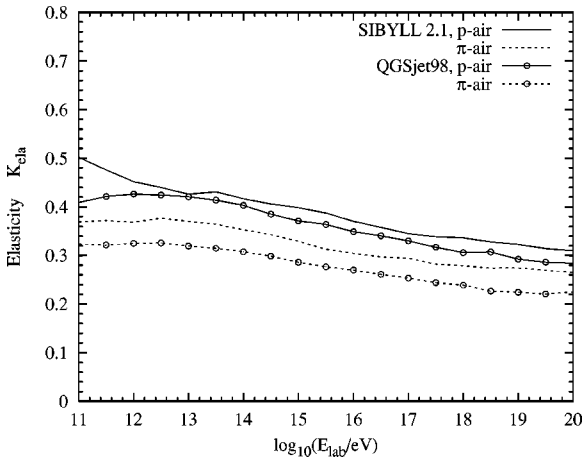

FIG. 6. Mean elasticity in proton-air collisions as predicted by QGSJET98 and SIBYLL 2.1 (see text).

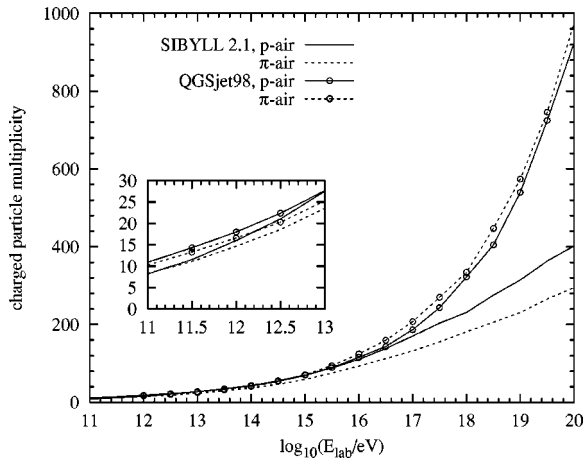

FIG. 7. Mean multiplicity of charged secondary particles produced in inelastic proton- and pion-air collisions.

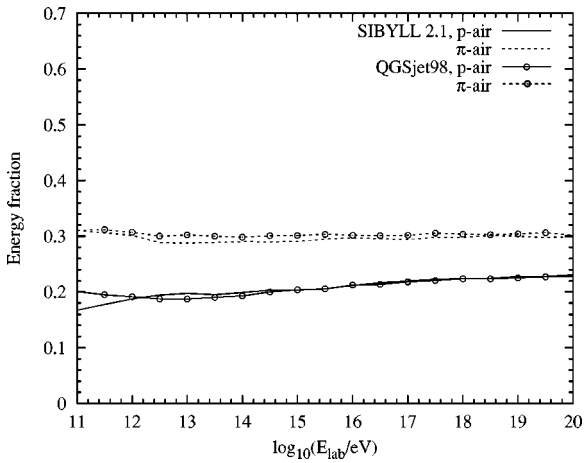

FIG. 8. Mean energy fraction carried by neutral pions, electrons and photons in inelastic proton- and pion-air collisions.

dicted by QGSJET98 and SIBYLL 2.1. We define the elasticity of an inelastic interaction (including diffraction dissociation) as $K_{\mathrm{el}}=E_{\mathrm{lead}}/E_{\mathrm{proj}}$ where E_{lead} is the energy of the most energetic hadron with a long lifetime (i.e. proton, neutron, Λ, and charged pions and kaons) and E_{proj} is the energy of the projectile particle. SIBYLL 2.1 consistently predicts more elastic collisions than QGSJET98 with a relative difference of up to 17%. Assuming similar other characteristics of hadronic interactions, a model with larger elasticity predicts air showers which develop deeper in the atmosphere.

Other important aspects relevant to air showers are the predicted multiplicity of secondaries and the energy fraction carried by neutral π^0's, which are closely related to the elasticity. Neutral pions decay immediately into two photons and feed the electromagnetic component of the shower. At the highest energies some neutral pions also interact hadronically because of the enormous time dilation. On the other hand, the charged particle multiplicity is a measure of how fast the initial energy is dissipated into many hadronic low-energy subshowers. It is also a good indicator for the muon multiplicity since the decaying charged pions are the primary source of muons.

Figure 7 shows the mean charged particle multiplicity in proton- and pion-air collisions as calculated with QGSJET98 and SIBYLL 2.1. QGSJET98 predicts a power-law-like increase of the number of secondary particles up to the highest energy. In contrast, the SIBYLL multiplicity exhibits a logarithmic growth similar to $\ln^2 s$ at high energy. In the energy region from 10^{13} to about 10^{16} eV both models predict the same multiplicity in p-air collisions. However the pion-air multiplicities are significantly different at all energies. In SIBYLL different parton densities are used for pions and protons. The currently implemented parametrizations from Glück et al. [47,48] predict fewer partons at low x in pions as compared to protons. The predicted secondary particle multiplicity is strikingly different at the highest energies. QGSJET98 predicts more than twice as many secondaries as SIBYLL. The multiplicity of neutral pions is closely linked to that of charged particles and hence shows qualitatively the same behavior.

The differences in multiplicity can again be qualitatively understood by considering Eq. (2). The minijet cross section predicted by perturbative QCD describes the inclusive cross section of minijet pairs. It does not specify how many minijets are produced per single hadron-hadron collision. The mean minijet multiplicity, $\langle n_{\mathrm{jet}}\rangle$, can only be calculated after knowing the inelastic cross section

$$\langle n_{\mathrm{jet}}\rangle=\sigma_{\mathrm{QCD}}/\sigma_{\mathrm{inel}}. \tag{10}$$

The larger multiplicity predicted by QGSJET stems both from the steeper energy dependence of its minijet cross section and from the more moderate energy dependence of its inelastic cross section. A detailed discussion of the relation between the minijet cross section and secondary particle multiplicity is given in [38].

Another difference is emphasized in the inset in Fig. 7. At low energy (i.e. 100 to 1000 GeV lab. energy) the multiplicity predicted for proton-air collisions is up to 25% lower in SIBYLL than in QGSJET. Whereas this difference is unimportant for electromagnetic shower variables, it becomes observable in the number of low-energy muons produced in the decay of charged pions and kaons.

Finally the mean energy fraction carried by π^0's, $e^{\pm}$'s and photons is shown in Fig. 8. Interestingly both models predict that the same fraction of the projectile energy is transferred to the electromagnetic shower component at high energy. However, the electromagnetic showers in a SIBYLL 2.1 simulation are more energetic and less numerous than with QGSJET98.

B. Shower size and depth of maximum

X_{max} and S_{max} are two typical shower parameters measured by fluorescence and Cherenkov light detectors in several experiments. Knowing the shower energy, the mean depth of shower maximum and its fluctuations can be used to infer the primary cosmic ray composition.

Figure 9 shows the average value of X_{max} as a function of primary energy for proton showers injected at a zenith angle $\theta=45°$. The lines were produced averaging X_{max} over 5000 showers. The predictions of SIBYLL 1.7, SIBYLL 2.1 and

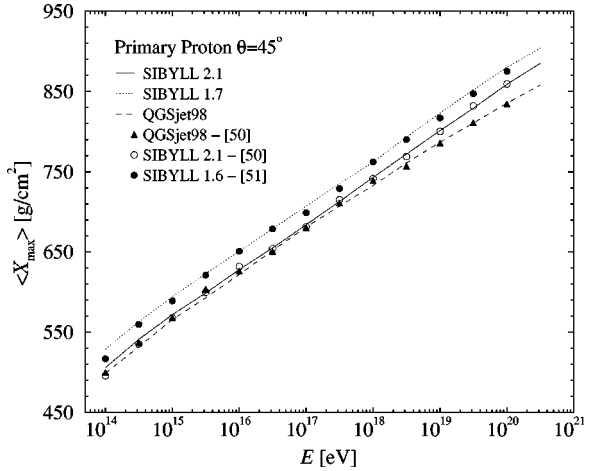

FIG. 9. Average depth of maximum $\langle X_{\max}\rangle$ of proton showers as a function of primary energy. The lines represent 5000 events generated by our one dimensional method, at $\theta=45°$, using SIBYLL 1.7 (dotted), SIBYLL 2.1 (solid) and QGSJET98 (dashed). The symbols show the values of $\langle X_{\max}\rangle$ averaged over 500 showers obtained with CORSIKA using the thinning procedure.

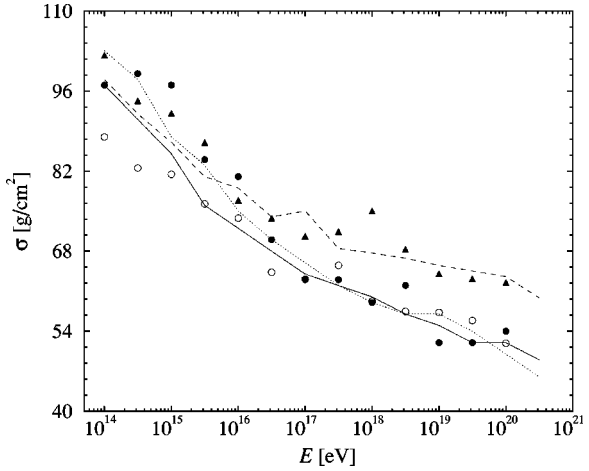

FIG. 10. Fluctuation of the position of the shower maximum, $\sigma=\sqrt{\langle X_{\max}^2\rangle-\langle X_{\max}\rangle^2}$. The curves have the same meaning as in Fig. 9.

QGSJET98 are shown. The first important feature is that SIBYLL 2.1 predicts smaller $\langle X_{\max}\rangle$ values than SIBYLL 1.7 by about 22 g/cm^2 from 10^{14} to 3×10^{20} eV. The predictions of SIBYLL 2.1 are closer to the values produced by QGSJET98. In fact, at energies below about 3×10^{17} eV the difference is smaller than 10 g/cm^2 and it increases with energy up to a maximum of 27 g/cm^2 at 3×10^{20} eV. QGSJET98 predicts values of $\langle X_{\max}\rangle$ systematically smaller than the ones produced by both versions of SIBYLL. This is due to the much higher average particle multiplicity generated by QGSJET98 and the lower elasticity compared to SIBYLL. These two features are responsible for the accelerated shower development in QGSJET98. Although the proton-air cross section in SIBYLL 2.1 is larger than the one predicted by QGSJET98 by 90 mb at 10^{20} eV, the larger multiplicity and smaller elasticity of the latter still dominate, producing a smaller $\langle X_{\max}\rangle$.

The width of the $X_{\max}$ distribution is a measure of the fluctuations of the position of the shower maximum. As shown in Fig. 10, the fluctuations become less important at very high energy. First of all, the fluctuations due to the position of the first interaction point are smaller at high energy due to the large cross section (small mean free path). Second, the large multiplicity of secondary particles produces a correspondingly larger number of subshowers. Individual subshowers will show considerable profile fluctuations as observed at lower energy, however, due to their large number the total shower profile exhibits much smaller fluctuations.

We have verified that the LPM effect [28–30] does not affect $\langle X_{\max}\rangle$ for proton energies below 3×10^{20} eV in agreement with [49]. The values of $\langle X_{\max}\rangle$ in proton showers at energy 3×10^{20} and in proton showers at the same energy but with the LPM artificially ''turned off'' are equal within $\sim1\%$. The large multiplicity of hadronic interactions at energies above the scale at which the LPM is important, is largely responsible for this small difference, because it reduces the energy of the neutral pions whose decays are the dominant channel for production of high energy photons in the shower. Neutral pions then do not produce photons energetic enough to show strong LPM characteristics. Even if a high energy neutral pion is created, for instance in diffractive interactions in which the multiplicity is low, at energies above $\sim10^{19}$ eV interactions of neutral pions dominate over decay and hence the production of high energy photons is suppressed [50].

Numerical values of $\langle X_{\max}\rangle$ and $\langle S_{\max}\rangle$ are presented in Table II for vertical proton induced showers. A comparison between $\langle X_{\max}\rangle$ in this table and in Fig. 9 reveals its weak dependence on the zenith angle in the angular range $\theta=0°-45°$. $\langle X_{\max}\rangle$ is fairly insensitive to changes in atmospheric density profile from $\theta=0°$ to $\theta=45°$ and hence it is approximately the same when expressed in g/cm^2. $\langle S_{\max}\rangle$ also shows a weak dependence on the zenith angle and it is remarkably independent of the hadronic interaction models adopted in this work. SIBYLL 2.1 produces $\langle S_{\max}\rangle$ values smaller than those predicted by SIBYLL 1.7 by 1% in the whole energy range shown in the table. An interesting aspect about the behavior of $S_{\max}/E$ with primary energy is that it increases up to energies of $\sim10^{17}$ eV and decreases after that for all three models.

In Figs. 9 and 10 we compare our predictions for proton showers to those obtained in the framework of the CORSIKA code using similar (or identical) hadronic interaction models [25,51,52]. Each of the points generated with CORSIKA in Figs. 9 and 10, represents the mean value of $X_{\max}$ over 500 showers using the thinning procedure. The values of $\langle X_{\max}\rangle$ and σ calculated by both codes for the same models are in very good agreement [40], within the larger statistical uncertainty of this particular CORSIKA calculation. This provides us a further check on the validity of the hybrid simulation method.

Figure 11 shows the distribution of $S_{\max}$ normalized by the primary energy in GeV. The top (bottom) histogram represents 5000 proton-induced vertical showers at 1 EeV (100

TABLE II. Mean depth of shower maximum development, $\langle X_{\max}\rangle$, and shower size at depth of maximum $\langle S_{\max}\rangle$, in proton-initiated shower with incident zenith angle $\theta=0°$. Each energy represents 5000 showers simulated with the hybrid method using SIBYLL 1.7, SIBYLL 2.1, and QGSJET98. The width of the corresponding distributions is given in parentheses.

Model	SIBYLL 1.7		SIBYLL 2.1		QGSJET98	
lg(E/eV)	$\langle X_{\max}\rangle$[g/cm^2]	$\langle S_{\max}\rangle/E$[GeV^{-1}]	$\langle X_{\max}\rangle$[g/cm^2]	$\langle S_{\max}\rangle/E$[GeV^{-1}]	$\langle X_{\max}\rangle$[g/cm^2]	$\langle S_{\max}\rangle/E$[GeV^{-1}]
14.0	530 (101)	0.691 (1.10×10^{-1})	507 (96)	0.688 (1.03×10^{-1})	499 (95)	0.685 (9.93×10^{-2})
15.0	592 (86)	0.719 (8.44×10^{-2})	571 (82)	0.719 (7.63×10^{-2})	565 (86)	0.724 (7.06×10^{-2})
16.0	647 (72)	0.735 (6.07×10^{-2})	626 (71)	0.734 (5.57×10^{-2})	625 (78)	0.736 (5.25×10^{-2})
17.0	706 (64)	0.739 (4.33×10^{-2})	684 (64)	0.737 (4.04×10^{-2})	677 (70)	0.738 (3.75×10^{-2})
18.0	760 (57)	0.737 (3.10×10^{-2})	740 (58)	0.734 (2.97×10^{-2})	730 (66)	0.728 (2.85×10^{-2})
19.0	822 (55)	0.723 (2.80×10^{-2})	799 (55)	0.718 (2.56×10^{-2})	785 (66)	0.708 (2.36×10^{-2})
20.0	878 (51)	0.694 (3.46×10^{-2})	856 (51)	0.690 (3.43×10^{-2})	832 (62)	0.683 (2.85×10^{-2})
20.5	901 (46)	0.671 (4.29×10^{-2})	880 (47)	0.666 (3.98×10^{-2})	853 (56)	0.662 (3.55×10^{-2})

EeV), calculated using SIBYLL 1.7, SIBYLL 2.1 and QGSJET98. The numerical values of $\langle S_{\max}\rangle/E$ are shown in Table II. The distribution of $S_{\max}/E$ is clearly not symmetric around the most likely value. This is a common feature of the three models and reflects the asymmetric fluctuations of the various interaction points and secondary particle multiplicities.

Figure 12 shows the distribution of $X_{\max}$, for the same shower initial parameters as in Fig. 11. The distribution has an asymmetric shape with a long tail at large values of $X_{\max}$. At both energies the tendency of QGSJET98 to predict lower values of $X_{\max}$ is clearly visible. The difference is more apparent when compared to the distribution obtained for SIBYLL 1.7. The distribution of $X_{\max}$ also reflects the larger fluctuations predicted by QGSJET98 compared to SIBYLL.

The fluctuations in $X_{\max}$ are directly related to the relative fraction of diffraction dissociation events generated in SIBYLL and QGSJET. In particular showers which develop very deep in the atmosphere are typically those with a diffractive first interaction. Inelastic diffraction in proton-air collisions can be subdivided into coherent and incoherent diffraction. The latter process corresponds to the interaction

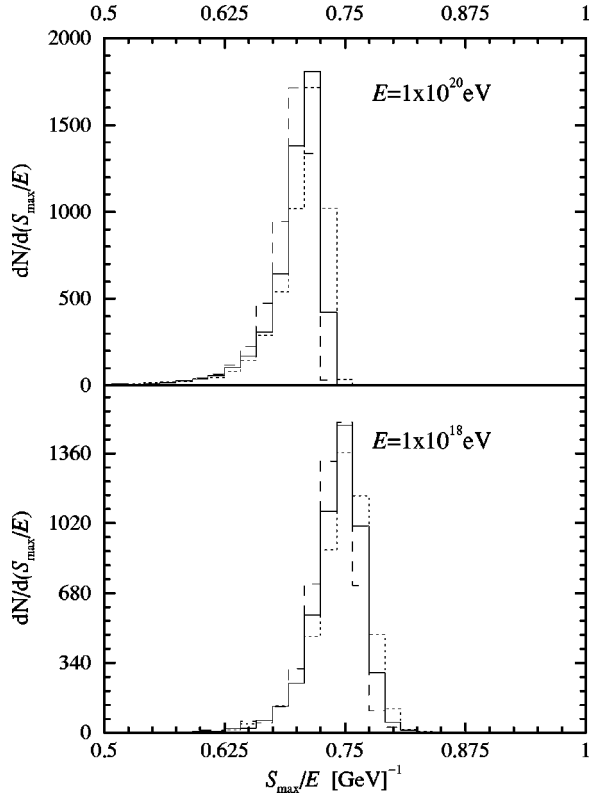

FIG. 11. Distribution of $S_{\max}$ normalized by the primary energy in GeV. Results are shown for 5000 primary proton showers of energies 10^{18} eV (bottom panel) and 10^{20} eV (top panel), with zenith angle $\theta=0°$ calculated with the hybrid method using SIBYLL 1.7 (dotted), SIBYLL 2.1 (solid), and QGSJET98 (dashed).

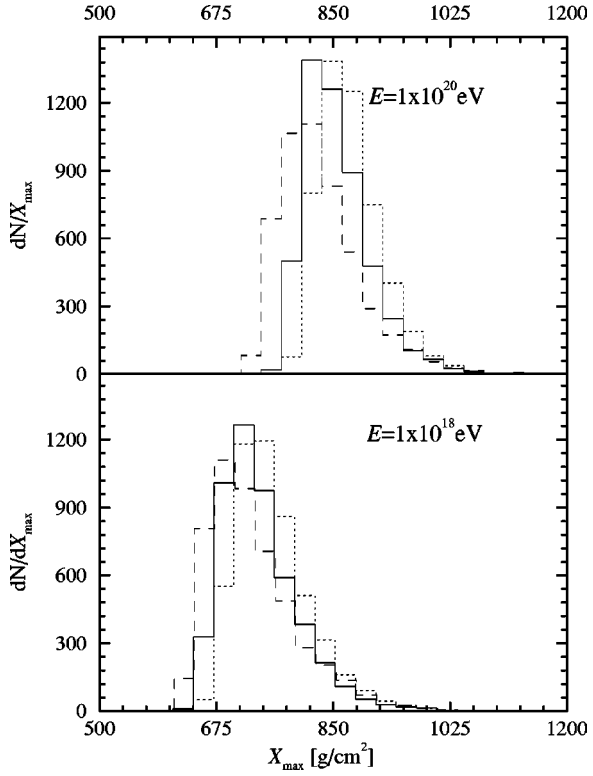

FIG. 12. Distribution of $X_{\max}$. Results are shown for 5000 vertical showers generated by primary protons of energies 10^{18} eV (bottom panel) and 10^{20} eV (top panel) calculated with the hybrid method using SIBYLL 1.7 (dotted), SIBYLL 2.1 (solid), and QGSJET98 (dashed).

of the projectile with a single nucleon of the target nucleus and is therefore completely analogous to diffraction in proton-proton collisions. As a multi-channel eikonal model [53] SIBYLL 2.1 predicts a growth of the cross section for diffraction dissociation in proton-proton collisions like $\ln s$ which means that the fraction of low-multiplicity events decreases at high energy as $1/\ln s$ [54]. In contrast, in QGSJET the fraction of diffractive events is essentially energy independent (more precisely proportional to the ratio of the elastic and inelastic cross sections) because it is based on the quasi-eikonal approximation [55]. From theoretical grounds the quasi-eikonal approximation is expected to overestimate the diffractive cross section at high energy as it does not implement the black disk limit (for a discussion of the black disk limit see, for example, [54]). On the other hand QGSJET accounts also for coherent diffraction which is neglected in SIBYLL.

C. Elongation rate

The elongation rate is defined as [23,24]

$$D_{10}=\frac{d\langle X_{\max}\rangle}{d\lg E}. \tag{11}$$

It describes the energy-dependence of the position of the shower maximum. The elongation rate reflects changes in the cosmic ray composition as well as features of hadronic interaction at high energy. Our interest here is in the relation between elongation rate and hadronic interactions.

Most of the charged particles in the shower are electrons and positrons with energies near the critical energy (81 MeV in air) from electromagnetic subshowers initiated by photons from π^0-decay. The mean depth of maximum for an electromagnetic shower initiated by a photon with energy E_γ is [56]

$$\langle X^{\rm em}_{\max}(E_\gamma)\rangle = X_0 \ln E_\gamma + C \tag{12}$$

where $X_0 \approx 37$ g/cm^2 is the radiation length in air. The elongation rate for an electromagnetic shower is thus $D^{\rm em}_{10} = \ln(10)\times X_0 \approx 85$ g/cm^2.

A proton-initiated shower consists of a hadronic core feeding the electromagnetic component primarily through π^0 production. In the approximation of a hadronic interaction model that obeys Feynman scaling with energy-independent cross sections, the energy splitting in the hadronic skeleton of the shower is independent of energy (i.e. it scales with energy). As a consequence, since the electromagnetic component is dominated by the earliest (i.e. most energetic) generations of hadronic interactions, under these assumptions the elongation rate of the hadronic shower is also $D^{\rm em}_{10}$. In general, for an incident nucleus of mass A and total energy E_0 (including protons with $A=1$) the depth of maximum is

$$\langle X_{\max}\rangle = X_0 \ln(E_0/A) + \lambda_A, \tag{13}$$

where λ_A is the interaction length of the primary particle. If the composition changes with energy, then $\langle A\rangle$ depends on energy and the elongation rate changes accordingly.

In qualitative analyses of the role of hadronic interactions in air shower development, an approach analogous to the treatment of nuclei has often been used. The depth of maximum for a proton shower is expressed as

$$\langle X^{\rm had}_{\max}(E)\rangle = \langle X^{\rm em}_{\max}(E/\langle n\rangle)\rangle + \lambda_N, \tag{14}$$

where $\langle n\rangle$ is related to the multiplicity of secondaries in the high-energy hadronic interactions in the cascade. The situation is, however, essentially more complicated than for a primary nucleus in which the energy is to a good approximation simply divided into A equal parts. In a hadronic cascade instead there is a hierarchy of energies of secondary particles in each interaction, and a similar (approximately geometric) hierarchy of interaction energies in the cascade. In this case $\langle n\rangle$ has to be understood as some kind of ''effective'' multiplicity, which does not have a straightforward definition in general.

The elongation rate derived from Eq. (14) is

$$\frac{d\langle X^{\rm had}_{\max}(E)\rangle}{d\lg E} = \ln(10) X_0 \left[1 - \frac{d\ln\langle n\rangle}{d\ln E}\right] + \frac{d\lambda_N}{d\lg E}, \tag{15}$$

which corresponds to the form given by Linsley and Watson [24],

$$D_{10} = \ln(10) X_0 (1 - B_n - B_\lambda), \tag{16}$$

with

$$B_n = \frac{d\ln\langle n\rangle}{d\ln E}, \quad B_\lambda = -\frac{\lambda_N}{X_0}\frac{d\ln\lambda_N}{d\ln E}. \tag{17}$$

For a hadronic interaction model with a multiplicity dependence of $\langle n\rangle = n_0 E^\delta$ one gets $B_n = \delta$ *provided* all secondaries having the same energy, which is not the case.

Because Eq. (16) is often used to estimate the elongation rate (see, for example, [57]), it is worthwhile to compare our results with this parametrization. Figure 13 shows the elongation rate for SIBYLL and QGSJET showers as derived from the detailed shower simulation. All the models show an initial decline from the low-energy scaling regime as expected. Then, above 10^{15} eV the elongation rate for SIBYLL is nearly constant while that for QGSJET continues to decline. In addition SIBYLL 1.7 has a sharp drop of the elongation rate at ultrahigh energy, which we explain below. In contrast, if we differentiate the curves in Figs. 5 and 7 for cross section and multiplicity and calculate the elongation rate from Eq. (16), using the assumption of equal sharing of energy among the secondaries, we get completely misleading results, particularly at low energy. For example, for QGSJET the predicted elongation rate is about 60 g/cm^2 over the entire energy range. The situation is similar for showers simulated with SIBYLL 2.1.

The use of the total particle multiplicity for $\langle n\rangle$ is not so bad at high energy because the scaling violation is fully developed in the high energy part of the shower. However, it is

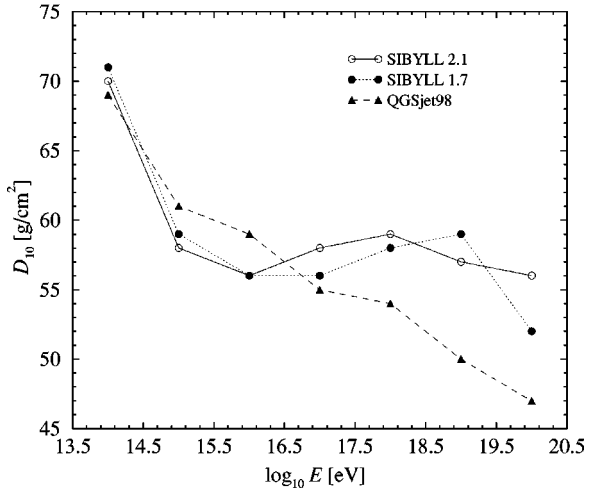

FIG. 13. Elongation rates, $d\langle X_{\max}\rangle/d\lg E$, calculated numerically using showers simulated with the hybrid method (see text).

important to note that in Eq. (16) the violation of Feynman scaling and the energy-dependence of the cross sections are taken into account only for the first interaction. All subsequent hadronic interactions are assumed to be characterized by Feynman scaling and constant interaction cross sections. Thus Eq. (16) is expected to be a good approximation only in an intermediate energy range around $10^{15}-10^{16}$ eV.

At higher energy the energy-dependence of the subsequent hadronic interactions becomes important. As an illustration, we consider a toy model in which all final state particles of the first proton interaction in air are charged pions and have the same energy. At high energy all pions will interact before decaying. As a first approximation we can write

$$\langle X^{\rm had}_{\max}(E)\rangle = \langle X^{\rm had}_{\max}(E/\langle n\rangle)\rangle + \lambda_N, \tag{18}$$

where now the position of maximum of pion induced secondary showers is written on the r.h.s. Using Eq. (15) to describe the pion showers one gets for the elongation rate of the entire shower

$$\frac{d\langle X^{\rm had}_{\max}(E)\rangle}{d\lg E} = \ln(10)X_0\left[1-\frac{d\ln\langle n(E)\rangle}{d\ln E} - \frac{d\ln\langle n[E/n(E)]\rangle}{d\ln E}\right] + \frac{d\lambda_N}{d\lg E} + \frac{d\lambda_\pi}{d\lg E}. \tag{19}$$

In a model with a power-law increase of the multiplicity with index δ this simplifies to

$$\frac{d\langle X^{\rm had}_{\max}(E)\rangle}{d\lg E} = \ln(10)X_0[1-2\delta+\delta^2] + \frac{d\lambda_N}{d\lg E} + \frac{d\lambda_\pi}{d\lg E}. \tag{20}$$

Using again the cross sections and multiplicities shown in Figs. 5 and 7 one gets elongation rates of about 43 and 56 g/cm^2 for QGSJET and SIBYLL , respectively. Given the simplicity of the model the predictions are remarkably close to the results of the full simulation above 10^{19} eV. This could be the result of a cancellation of two effects: on one hand only two successive hadronic interactions were assumed to be energy-dependent and, on the other hand, the scaling violation in these interactions was overestimated by using the total particle multiplicity in Eq. (19) and the uniform energy sharing.

Finally it should be mentioned that the sudden drop of the elongation rate of the showers simulated with SIBYLL 1.7 is due to the onset of the interaction of neutral pions. At energies above $10^{19.5}$ eV a substantial number of π^0's does not decay but interacts because of the enormous Lorentz dilation. This effect reduces the mean energy of the particles which feed the electromagnetic component of the shower. The change in elongation rate is most prominent in SIBYLL 1.7 because it generates more fast (interacting) neutral pions.

D. Number of muons

The number of muons in a shower is an important observable which depends strongly on the mass of the primary particle and is used in the studies of the elemental composition of cosmic rays. It also directly reflects the hadronic component of the shower and hence it is a sensitive probe of the hadronic interactions.

We have calculated the average number of muons at sea level ($\langle N_\mu\rangle$) with energies above $E_\mu^{\rm thr}=0.3,1,3,10$ and 30 GeV, in proton-initiated showers at zenith angle $\theta=0°$ ($\theta=45°$) for the hadronic models SIBYLL 1.7, SIBYLL 2.1, and QGSJET98. Figure 14 shows the energy dependence of the average number of muons normalized to the primary energy for the three models. $\langle N_\mu\rangle$ follows approximately a simple

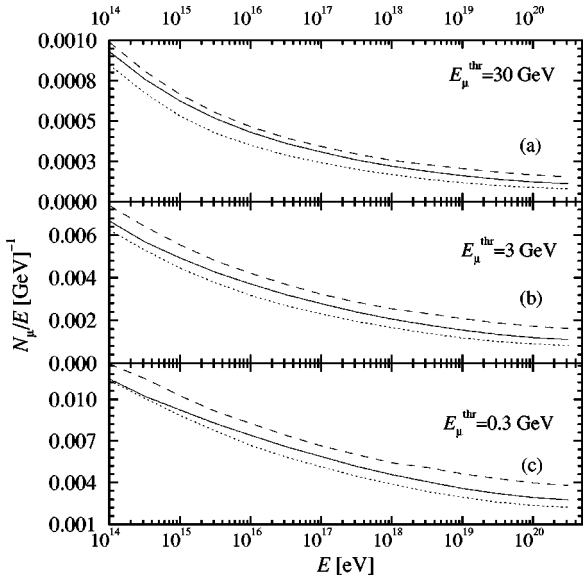

FIG. 14. Average number of muons at sea level $\langle N_\mu\rangle$, obtained in proton showers with zenith angle $\theta=0°$. Each energy represents 5000 showers simulated with the hybrid method. The solid (dotted) line represents the values obtained with SIBYLL 2.1 (SIBYLL 1.7), while the dashed line illustrates the values for QGSJET98. Panels (a), (b) and (c) show the average number of muons with energy above 30 GeV, 3 GeV and 0.3 GeV respectively.

TABLE III. Parameters α and E_c obtained by fitting the number of muons in vertical showers at sea level using a power law of the form $N_\mu=(E/E_c)^\alpha$. The numerical values of the parameters are presented for the three hadronic models and for muons with energy above 0.3, 1, 3, 10 and 30 GeV.

Model	SIBYLL 1.7					SIBYLL 2.1					QGSJET98				
$E_\mu^{\rm thr}$ [GeV]	0.3	1	3	10	30	0.3	1	3	10	30	0.3	1	3	10	30
α	0.886	0.877	0.869	0.857	0.846	0.901	0.893	0.884	0.872	0.861	0.920	0.913	0.904	0.893	0.882
E_c [GeV]	35	43	67	162	594	39	47	70	161	555	44	53	79	182	638

power law $(E/E_c)^\alpha$ for energies above $\sim 10^{14}$ eV.

This can be understood on the basis of Heitler's model [58] (see also the discussion in [59]) by assuming that each hadronic interaction produces in average $\langle n_{\rm tot}\rangle$ secondaries of approximately the same energy. The multiplication of the number of charged pions in a shower continues until the pions reach a critical energy, E_c, at which they are assumed to decay. After N generations (i.e. subsequent interactions) the energy of the pions reaches the critical energy $E_c = E/\langle n_{\rm tot}\rangle^N$. The number of muons from decaying charged pions is thus $N_\mu=\langle n_{\pi^\pm}\rangle^N$. Eliminating N gives

$$N_\mu=\left(\frac{E}{E_c}\right)^\alpha, \alpha=\frac{\ln\langle n_{\pi^\pm}\rangle}{\ln\langle n_{\rm tot}\rangle}, \tag{21}$$

which is the well-known power-law found in data. The index α can be calculated by using $\langle n_{\pi^\pm}\rangle\approx\frac{2}{3}\langle n_{\rm tot}\rangle$, which gives values for α in the range from 0.85 to 0.92. (Assuming that the charged pion multiplicity is less than 2/3 of the total multiplicity decreases the values predicted for α.)

Over the entire energy range from 10^{14} eV to more than 10^{20} eV a single power law parametrization can be used to describe the muon multiplicities for all the energy threshold considered here. In Tables III and IV we show the corresponding fit parameters for showers of 0° and 45° zenith angle, respectively. As expected the critical energy increases with the muon threshold energy. The energy-dependence of the muon multiplicity is the steepest for low-energy muons. For a given muon energy threshold, the numerical value of α tends to be the highest for the QGSJET98 model.

Already from the simple model discussed above it is clear that the power-law index should be energy-dependent because the multiplicity of the secondary particles increases with energy. Indeed, a careful inspection of the energy dependence of $\langle N_\mu\rangle$ shows that the power law index α increases with the primary energy. However, the observed relative deviation from a single power law is always less than 15%. It is the regularity of this deviation and the aforementioned physics motivation which makes it worthwhile to consider the following, alternative parametrization.

The power-law index is taken to be energy-dependent with

$$\alpha(E)=\left[1+\frac{\ln(3/2)}{\ln\langle n_{\rm eff}\rangle}\right]^{-1}, \tag{22}$$

where $n_{\rm eff}$ is the geometric average of the charged pion multiplicity of N successive hadronic interactions. By construction this effective multiplicity has a weak energy dependence, which we approximate by

$$\ln\langle n_{\rm eff}\rangle\approx n_0+n_1\ln\left(\frac{E}{E_0}\right), \quad E_0=10^{14}\ \text{eV}. \tag{23}$$

To make the numerical values of $\alpha(E)$ more transparent we express the parameters n_0 and n_1 in terms of power-law indices $\alpha_0=\alpha(E_0)$ and $\alpha_1=\alpha(E_1=10^{20}\text{eV})$

$$n_0=\frac{\alpha_0}{1-\alpha_0}\ln(3/2) \tag{24}$$

$$n_1=\frac{\ln(3/2)}{\ln(E_1/E_0)}\left[\frac{\alpha_1}{1-\alpha_1}-\frac{\alpha_0}{1-\alpha_0}\right]. \tag{25}$$

This alternative muon multiplicity parametrization has only three free parameters, the indices α_0, α_1 and the critical energy E_c. It gives considerably better fits to the simulation data than the single power-law parametrization (21). The numerical values obtained by fitting the output of the hybrid simulations are shown in Tables V and VI. The relative uncertainties of the parameters α_0, α_1 are about 1% and 10–15 % for E_c.

The QGSJET98 model shows the biggest change of the power law index from α_0 to α_1. Muon production in

TABLE IV. Parameters α and E_c obtained by fitting the number of muons in showers with $\theta=45°$ at sea level using a power law of the form $N_\mu=(E/E_c)^\alpha$. The numerical values of the parameters are presented for the three hadronic models and for muons with energy above 0.3, 1, 3, 10 and 30 GeV.

Model	SIBYLL 1.7					SIBYLL 2.1					QGSJET98				
$E_\mu^{\rm thr}$ [GeV]	0.3	1	3	10	30	0.3	1	3	10	30	0.3	1	3	10	30
α	0.891	0.886	0.877	0.867	0.853	0.902	0.897	0.890	0.878	0.865	0.921	0.916	0.909	0.899	0.887
E_c [GeV]	65	72	94	195	562	67	74	96	185	523	77	83	107	209	607

TABLE V. Parameters α_0, α_1 and E_c obtained by fitting the number of muons in vertical showers at sea level to Eq. (22). The numerical values of the parameters are presented for the three hadronic models and for muons with energy above 0.3, 1, 3, 10 and 30 GeV.

Model	SIBYLL 1.7					SIBYLL 2.1					QGSJET98				
$E_\mu^{\rm thr}$ [GeV]	0.3	1	3	10	30	0.3	1	3	10	30	0.3	1	3	10	30
α_0	0.858	0.838	0.819	0.780	0.745	0.887	0.870	0.850	0.820	0.787	0.855	0.834	0.809	0.775	0.736
α_1	0.874	0.861	0.849	0.827	0.809	0.895	0.883	0.870	0.852	0.834	0.892	0.879	0.864	0.846	0.828
E_c [GeV]	26	28	39	74	238	33	36	49	97	291	22	23	29	57	179

SIBYLL 2.1 is the closest to a simple power law. The general trend for all three models is that the power law index decreases with the muon threshold energy.

The absolute number of muons differs from model to model. SIBYLL 2.1 produces more muons than SIBYLL 1.7 but still less than QGSJET98 at all energies. The differences between the three models increase with energy and reach maximum at 10^{20} eV. Table VII gives the ratios of $\langle N_\mu \rangle$ generated by SIBYLL 1.7 and QGSJET98 at sea level to those generated by SIBYLL 2.1 in vertical showers at primary energies of 10^{15} eV and 10^{20} eV.

It is interesting to observe the dependence of these differences on the muon threshold energy. While for SIBYLL 1.7 the ratio decreases monotonically with the threshold energy, the QGSJET98/SIBYLL 2.1 ratio shows a more complex behavior. The enhanced production of low energy muons in QGSJET98 is related to the higher charged multiplicity of the model in the 100–1000 GeV range. The differences between the two models decrease for $E_\mu^{\rm thr}$ of 30 GeV.

The number of muons at sea level is sensitive to the incident zenith angle. Two competing processes—muon production and muon energy loss and decay—determine the dependence on the zenith angle. With increasing zenith angle both the grammage in which showers develop and the distance to the observation level increase. Some additional muons are generated in inclined showers due to the larger number of interactions, but also a large fraction of the low energy muons (below $\sim$3 GeV) decay before reaching sea level. Decays win the competition and the number of low energy muons decreases with the zenith angle. At energies above $\sim$10 GeV, however, most of the muons cross the whole atmosphere without decaying, and their number at sea level is less sensitive to the injection angle.

This behavior is illustrated in Fig. 15 which shows the distribution of the number of muons at sea level for different $E_\mu^{\rm thr}$ and zenith angles of 0° and 45°. Each histogram represents 5000 showers initiated by primary protons at 1 EeV using the SIBYLL 2.1 model.

At energy above 30 GeV practically all muons cross the atmosphere without decaying. The difference in the number of muons above 30 GeV between the two zenith angles, depicted in Fig. 15, is then determined by muon production. At large zenith angles shower particles travel for a longer time in a more tenuous atmosphere and hence the charged pions have a smaller probability of interaction. As a result more muons are produced at $\theta=45°$ than at $\theta=0°$.

SIBYLL 2.1 and QGSJET98 predict similar fluctuations in the number of muons. At $E=10^{18}$ eV the width of the shower distribution in muons obtained with QGSJET98 is only $\sim$7% larger than in SIBYLL 2.1 for all muon energy thresholds. The difference in the widths at 10^{18} eV as obtained with QGSJET98 and SIBYLL 1.7 is larger and increases from $\sim$17% at $E_\mu^{\rm thr}=0.3$ GeV to $\sim$27% at $E_\mu^{\rm thr}=30$ GeV.

IV. SUMMARY AND OUTLOOK

We have presented an efficient, one-dimensional hybrid method to simulate the development of extensive air showers. The combination of Monte Carlo techniques for the interactions of the shower particles above a certain hybrid energy threshold with a presimulated library of pion-induced showers, allows us to simulate the development of large statistical samples of air showers up to the highest energies observed.

Previously developed hybrid methods use the average longitudinal development to describe the numerous subthreshold showers and are usually limited to the calculation of the total number of electromagnetic particles. In this paper we have presented a method that accounts for fluctuations in the shower development as well as the correlations between the different parameters describing the electromagnetic and muon components of EAS.

We have simulated showers using the hybrid method with and without accounting for fluctuations in the subshower development, and studied the role of the fluctuations on the electromagnetic component. Our approach gives a better de-

TABLE VI. Parameters α_0, α_1 and E_c obtained by fitting the number muons in inclined showers ($\theta=45°$) at sea level to Eq. (22). The numerical values of the parameters are presented for the three hadronic models and for muons with energy above 0.3, 1, 3, 10 and 30 GeV.

Model	SIBYLL 1.7					SIBYLL 2.1					QGSJET98				
$E_\mu^{\rm thr}$ [GeV]	0.3	1	3	10	30	0.3	1	3	10	30	0.3	1	3	10	30
α_0	0.873	0.863	0.842	0.819	0.764	0.892	0.883	0.867	0.839	0.802	0.858	0.848	0.828	0.794	0.751
α_1	0.884	0.876	0.863	0.849	0.821	0.898	0.891	0.881	0.863	0.842	0.895	0.888	0.876	0.858	0.837
E_c [GeV]	54	57	66	124	255	61	64	76	128	304	41	42	48	78	189

TABLE VII. Ratios of $\langle N_\mu \rangle$ at sea level generated in vertical showers by SIBYLL 1.7 and QGSJET98 to those generated by SIBYLL 2.1 ($\equiv 1$).

E [eV]	10^{15}			10^{20}		
$E_\mu^{\rm thr}$ [GeV]	0.3	3	30	0.3	3	30
SIBYLL 1.7	0.96	0.92	0.87	0.83	0.81	0.78
QGSJET98	1.11	1.12	1.06	1.37	1.41	1.35

scription of the $S_{\rm max}$ distributions (at the level of $\sim 3-5\,\%$), and of the tails of the shower size at sea level and $X_{\rm max}$ distributions. We could not compare the muon distributions because they were not available in the old hybrid method [16]. We believe however that a good description of the muon numbers requires an accurate account of the fluctuations at low energies.

By comparing direct simulations with hybrid-simulated showers we have determined that the correlation between the hadronic and the electromagnetic component is also well reproduced with our method. In particular the hybrid method correctly describes the correlation between the number of muons and the shower size at observation level, which is of special relevance to studies of the cosmic ray composition.

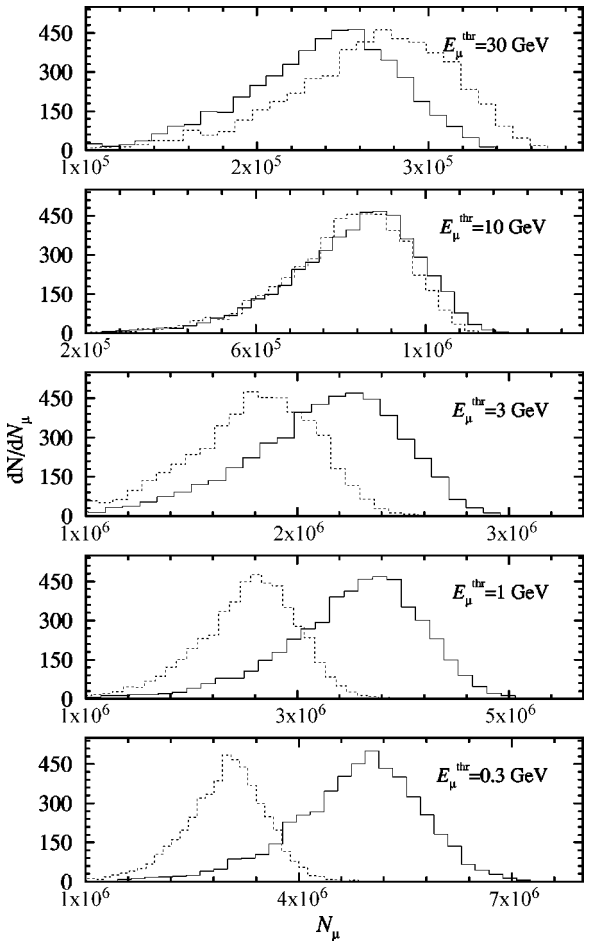

FIG. 15. Shower distribution in number of muons at sea level. The results are obtained for 5,000 primary proton showers of energy 10^{18} eV for different muon energy thresholds. The solid line represents vertical showers, while the dotted line illustrates showers with zenith angle $\theta = 45°$. All showers were simulated using SIBYLL 2.1.

We have studied the influence of different hadronic interaction models, namely SIBYLL 1.7, SIBYLL 2.1 and QGSJET-98, on shower observables which are relevant for the determination of the energy and chemical composition of the primary cosmic ray flux. We have presented average values of $X_{\rm max}$, $S_{\rm max}$ and the number of muons above 0.3, 1, 3, 10 and 30 GeV at sea level, as well as the fluctuations of these quantities. The mean muon multiplicities were analyzed with two different models: (i) a simple power-law parametrization, which describes the simulation results with a relative accuracy of better than 10% (15% for $E_\mu^{\rm thr}=30$ GeV), and (ii) a model with a slowly changing power-law index, which gives an excellent description of the data. The relation between the features of the interaction models and the shower observables has been extensively discussed. We stress the influence of the different extrapolations of the hadronic models to the highest energies on the features of the electromagnetic and hadronic component of the shower, and the influence of the differences between the models on the number of muons predicted by them. Some of these differences exist already at low energies and affect the average numbers of low energy muons.

In QCD-inspired models such as SIBYLL and QGSJET the predictions on cross sections are inherently linked to the size of the Feynman scaling violation, and hence multiplicity, implemented in the model. A model with a steep energy-dependence of the hadron-air cross section is usually characterized by a moderate increase of the multiplicity. Concerning the position of the shower maximum, the effect of a large Feynman scaling violation (or a steeply rising multiplicity) is similar to that of a steeply rising cross section. This is the reason why the $\langle X_{\rm max} \rangle$ predictions of SIBYLL 2.1 and QGSJET98 are rather similar over a wide energy range. On the other hand, the number of muons at sea level reflects the multiplicity of low-energy hadrons produced in a shower but depends only weakly on the hadronic cross sections. Therefore, showers simulated with QGSJET produce consistently more low-energy muons than SIBYLL showers.

As another application of our method we have studied the influence of the multiplicity, inelasticity, proton-air cross section on the elongation rate of proton-initiated showers. We find that the elongation rate has a complex dependence on the scaling violation and cross section behavior of hadronic interaction models. Again, a steeply rising cross section leads to a decrease of the elongation rate qualitatively similar to a steeply rising multiplicity. Furthermore, a threshold-like behavior is observed at extremely high energy. The onset of the hadronic interaction of neutral pions, which always decay at low energy, leads to a significant decrease of the elongation rate.

In forthcoming work we will apply our hybrid method to the determination of the proton-air cross section in experiments that are able to measure the muon and electromagnetic components at fixed depth, as well as in experiments capable of measuring the distribution of $X_{\rm max}$. Furthermore, we will exploit the fastness of our method to simulate large statistical

samples of showers initiated by heavy nuclei, with the aim to predict observables that help in studying the composition of the cosmic ray flux.

ACKNOWLEDGMENTS

We are indebted to H.P. Vankov for making his LPM code available to us and for many discussions. We thank D. Heck for providing us with the values of $X_{\max}$ for CORSIKA. We also acknowledge fruitful discussions with D. Heck, P. Lipari, S. Ostapchenko, and T. Thouw. J.A.O. is supported by CAPES ''Bolsista da CAPES - Brasília/Brasil'' and acknowledges Bartol Research Institute for its hospitality. This research is supported in part by NASA Grant No. NAG5-10919. R.E., T.K.G. and T.S. are also supported by the U.S. Department of Energy Contract DE-FG02 91ER 40626. T.S. also acknowledges the hospitality of PCC, Collège de France and a grant from the Ministère de la Recherche of France. The simulations presented here were performed on Beowulf clusters funded by NSF Grant ATM-9977692.

[1] M. Nagano and A.A. Watson, Rev. Mod. Phys. **72**, 689 (2000).
[2] K. Kampert, J. Phys. G **27**, 1663 (2001).
[3] D.J. Bird *et al.*, Astrophys. J. **441**, 144 (1995).
[4] M. Takeda *et al.*, Phys. Rev. Lett. **81**, 1163 (1998).
[5] A.M. Hillas, Nucl. Phys. B (Proc. Suppl.) **52B**, 29 (1997).
[6] Y. Shirasaki and F. Kakimoto, Astropart. Phys. **15**, 241 (2001).
[7] J.N. Capdevielle, C. Le Gall, and K.N. Sanosian, Astropart. Phys. **13**, 259 (2000).
[8] M. Kobal, Astropart. Phys. **15**, 259 (2001).
[9] M. Risse, D. Heck, J. Knapp, and S. S. Ostapchenko, in *Proceedings of the 27th International Cosmic Ray Conference*, Hamburg, Germany, 2001, edited by K.-H. Kampert, G. Heinzelmann, and C. Spiering (Copernicus Gesellschaft, Katlemburg-Lindau, 2001), p. 522.
[10] L.G. Dedenko, Can. J. Phys. **46**, 178 (1968).
[11] N. N. Kalmykov, S. S. Ostapchenko, and K. Werner, in *Proceedings of the 27th International Cosmic Ray Conference*, (Ref. [9]), p. 443.
[12] A. Kirillov and I. Kirillov, in *Proceedings of the 27th International Cosmic Ray Conference*, (Ref. [9]), p. 483.
[13] A. Kirillov *et al.*, Izv. Ross. Akad. Nauk. (to be published).
[14] G. Bossard *et al.*, Phys. Rev. D **63**, 054030 (2001).
[15] J. Drescher and G. Farrar, talk given at Aspen Center for Physics 2002 Winter Conference, http://astro.uchicago.edu/~olinto/aspen/program
[16] T. K. Gaisser, P. Lipari, and T. Stanev, in *Proceedings of the 25th International Cosmic Ray Conference*, Durban, South Africa, 1997 (World Scientific, Singapore, 1997), Vol. 6, p. 281.
[17] T. Stanev and H.P. Vankov, Astropart. Phys. **2**, 35 (1994).
[18] T. Abu-Zayyad *et al.*, Nucl. Instrum. Methods Phys. Res. A **450**, 253 (2000).
[19] J. Cronin *et al.*, The Pierre Auger Project design report 2nd ed., available at Auger website www.auger.org (1995).
[20] O. Catalano, Nuovo Cimento Soc. Ital. Fis., C **24C**, 445 (2001).
[21] R.E. Streitmatter (OWL), in *Proceedings of the Workshop on Observing Giant Cosmic Ray Air Showers from* $>10^{20}$ *eV Particles from Space, College Park, MD*, edited by J. F. Krizmanic, J. F. Ormes, and R. E. Streitmatter, AIP Conf. Proc. No. 433 (AIP, Woodbury, NY, 1997), p. 95.
[22] M. Sasaki, in *Proceedings of the EHECR 2001, International Workshop on Extremely High Energy Cosmic Rays*, ICRR, Kashiwa, Japan, 2001 [J. Phys. Soc. Jpn. Suppl. B **70** (2001)].
[23] J. Linsley, in *Proceedings of the 15th International Cosmic Ray Conference*, Plovdiv, Bulgaria, 1977 (Bulgarian Academy of Sciences, Sofia, 1977), Vol. 12, p. 89.
[24] J. Linsley and A.A. Watson, Phys. Rev. Lett. **46**, 459 (1981).
[25] D. Heck, J. Knapp, J. N. Capdevielle, G. Schatz, and T. Thouw, Report FZKA 6019 (1998).
[26] S. E. Forsythe, *Smithsonian Physical Tables* (Smithsonian Institution Press, Washington, D.C., 1969).
[27] T. K. Gaisser, M. Shibata, and J. A. Wrotniak, Bartol Report No. 81-21 (1981).
[28] L.D. Landau and I.J. Pomeranchuk, Dokl. Akad. Nauk SSSR **92**, 535 (1953).
[29] L.D. Landau and I.J. Pomeranchuk, Dokl. Akad. Nauk SSSR **92**, 735 (1953).
[30] A.B. Migdal, Phys. Rev. **103**, 1811 (1956).
[31] S. R. Klein, in *Proceedings of the Workshop on Observing Giant Cosmic Ray Air Showers from* $>10^{20}$ *eV Particles from Space* (Ref. [21]), p. 132.
[32] H. P. Vankov (private communication).
[33] T. Stanev and H.P. Vankov, Phys. Rev. D **55**, 1365 (1997).
[34] T. K. Gaisser, *Cosmic Rays and Particle Physics* (Cambridge University Press, Cambridge, England, 1990).
[35] J. Alvarez-Muñiz, R. Engel, T. K. Gaisser, J. Ortiz, and T. Stanev (in preparation).
[36] R.S. Fletcher, T.K. Gaisser, P. Lipari, and T. Stanev, Phys. Rev. D **50**, 5710 (1994).
[37] R. Engel, T. K. Gaisser, P. Lipari, and T. Stanev, in *Proceedings of the 26th International Cosmic Ray Conference*, Salt Lake City, 1999, edited by D. Kieda, M. Salamon, and B. Dingus (AIP, Melville, NY, 2000), Vol. 1, p. 415.
[38] R. Engel, T. K. Gaisser, and T. Stanev, in *Proceedings of the 27th International Cosmic Ray Conference* (Ref. [9]), p. 431.
[39] N.N. Kalmykov, S.S. Ostapchenko, and A.I. Pavlov, Nucl. Phys. B (Proc. Suppl.) **52B**, 17 (1997).
[40] S. P. Swordy *et al.*, Astropart. Phys. (to be published).
[41] S. Ostapchenko, T. Thouw, and K. Werner, Nucl. Phys. B (Proc. Suppl.) **52B**, 113 (1997).
[42] J. Kwieciński and A.D. Martin, Phys. Rev. D **43**, 1560 (1991).
[43] H. Abramowicz and A. Caldwell, Rev. Mod. Phys. **71**, 1275 (1999).
[44] C. Furget, M. Buenerd, and P. Valin, Z. Phys. C **47**, 377 (1990).
[45] M.M. Block and R.N. Cahn, Rev. Mod. Phys. **57**, 563 (1985).
[46] M.M. Block, E.M. Gregores, F. Halzen, and G. Pancheri, Phys. Rev. D **60**, 054024 (1999).
[47] M. Glück, E. Reya, and A. Vogt, Eur. Phys. J. C **5**, 461 (1998).
[48] M. Glück, E. Reya, and I. Schienbein, Eur. Phys. J. C **10**, 313 (1999).
[49] A.N. Cillis, H. Fanchiotti, C.A. García Canal, and S.J. Sciutto, Phys. Rev. D **59**, 113012 (1999).

[50] J. Alvarez-Muñiz and E. Zas, Phys. Lett. B **434**, 396 (1998).
[51] D. Heck, astro-ph/0103073; and (private communication).
[52] C.L. Pryke, Astropart. Phys. **14**, 4 (2001).
[53] A.B. Kaidalov, Phys. Rep. **50**, 157 (1979).
[54] R. Engel, Nucl. Phys. B (Proc. Suppl.) **82**, 221 (2000).
[55] K.G. Boreskov, A.M. Lapidus, S.T. Sukhorukov, and K.A. Ter-Martirosyan, Yad. Fiz. **16**, 389 (1972).
[56] B. Rossi and K. Greisen, Rev. Mod. Phys. **13**, 240 (1941).
[57] C. Pajares, D. Sousa, and R.A. Vázquez, Phys. Rev. Lett. **86**, 1674 (2001).
[58] W. Heitler, *Quantum Theory of Radiation*, 2nd ed. (Oxford University Press, Oxford, 1944).
[59] J. Matthews in *Proceedings of the 27th International Cosmic Ray Conference*, (Ref. [9]), p. 261.